Excitation and temperature of extended gas in active galaxies

II. Photoionization models with matter-bounded clouds

Luc Binette[1]*, Andrew S. Wilson[2,3] and Thaisa Storchi-Bergmann[4]

[1] Observatoire de Lyon, UMR CNRS 5574, 9 av. Charles André, F-69561 Saint-Genis-Laval Cedex, France
[2] Space Telescope Science Institute, 3700 San Martin Drive, Baltimore, Maryland 21218, USA
[3] Astronomy Department, University of Maryland, College Park, MD 20742, USA
[4] Instituto de Fisica, UFRGS, Campus do Vale, 91500 Porto Alegre, RS, Brasil

Abstract. Recent reliable measurements of the weak lines of [O III]$\lambda4363$, He II $\lambda4686$ and [Ne V]$\lambda3426$ seen in emission in extended and nuclear regions of AGN (Storchi-Bergmann et al. 1996) are used to discriminate between different types of photoionization models. The sample comprises Seyferts and Narrow Line Radio Galaxies. A well known problem, the scatter and the extreme values of He II/Hβ encountered in the nuclei and extended regions, is solved in a similar fashion to Viegas & Prieto (1992) by considering two populations of ionized clouds: a matter-bounded (MB) component responsible for most of the He II emission, and an ionization-bounded (IB) component emitting low-to-intermediate excitation lines. A new sequence of photoionization calculations is thereby obtained by varying $A_{M/I}$, which is defined as the solid angle ratio occupied by the MB component relative to the IB component. In various line ratio diagrams, the $A_{M/I}$-sequence is compared to the traditional single component U-sequence in which one arbitrarily varies the relative intensity of the ionizing source. An original aspect of the new calculations is that the IB clouds are photoionized exclusively by the radiation which has filtered ('leaked') through the MB component. This situation could arise if, for example, the MB component is the low density 'halo' of a cloud, and the IB component the high density core. Such a filtered ionizing spectrum enlarges the range in He II/Hβ accessible to models without requiring changes in the spectral index of the ionizing source, which we fix at $\alpha=-1.3$. The main success of the model is that it provides a natural explanation for the newly found correlations between both the [O II]/[Ne V] and [O II]/[O III] ratio and the He II/Hβ ratio. On the other hand, the standard U-sequence cannot account for such correlations between the gaseous excitation and the He II/Hβ ratio. Furthermore, the so-called 'temperature problem' is solved with the $A_{M/I}$-sequence provided the thickness and the ionization parameter ($U_{MB} \gtrsim 0.03$) of the MB component are appropriately selected. Finally, the $A_{M/I}$-sequence produces much stronger high excitation lines of [Ne V] and C IV $\lambda\lambda1549$ than the U-sequence, in accordance with observations. The $A_{M/I}$-sequence predicts a temperature difference of 5 000 K between the T_{OIII} and T_{NII} temperatures while for the U-sequence this difference is less than 1 000 K. To the extent that 'cooling flows' and LINERs share the same excitation mechanism as our IB component (i.e. photoionization by an absorbed ionizing continuum), we predict a value of He II/H$\beta < 0.01$ while the U-sequence is charaterized by a value > 0.1.

Key words: galaxies: active – galaxies: Seyfert – line: formation – galaxies: ISM

1. Introduction

Modelling and interpretation of the so called Narrow Line Region (NLR) of active galactic nuclei is widely covered in the literature. Photoionization (defined broadly and including photoionizing shocks) is believed to be the dominant excitation mechanism although other mechanisms may also play a role (as reviewed in Viegas & de Gouveia Del Pino 1992: VGDP). The emission line region is, however, not confined to the unresolved inner nucleus but extends up to several kpc in Seyfert galaxies (hereafter Extended Narrow Line Region or ENLR; Unger et al. 1987; Haniff et al. 1991; Durret 1990) and up to 50 kpc and beyond in radio-galaxies (hereafter Extended Emission Line Region or EELR; Fosbury 1989; McCarthy 1993). Any understanding of the excitation and physical conditions in extended gas may also be helpful in modelling the low-to-intermediate density ($n < 10^7 \, \text{cm}^{-3}$) region of the spatially unresolved NLR. Studies of extended gas, however, are markedly facilitated by the fact that important geometrical parameters become available through imaging. Equally important is the lower density ($n < 10^3 \, \text{cm}^{-3}$; Morganti et al. 1991; Tadhunter et

1994), which simplifies multicomponent modeling since collisional deexcitation of the forbidden lines can be disregarded except for a few lines which become density indicators. Single component models (i.e. models with a single density n and a single ionization parameter U [defined as the ratio of the density of ionizing photons to the gas density, Eq. 1]) of the NLR, although broadly successful in fitting strong optical lines, are unsatisfactory in important aspects, as reviewed below (see also VGDP). Interestingly enough, the same inadequacies of models (as for the NLR) are found for the extended gas of the ENLR and EELR. In this paper, we argue that the next and simplest modification of the single component model is to consider two distinct populations of line emitting clouds. In particular, we propose a *variable* ratio of a matter-bounded component and an ionization-bounded component and show that such a model can resolve the remaining crucial problems pertaining to photoionization models. Let us review first the standard problems encountered in current photoionization models.

1.1. The nuclear region: the NLR

There are three serious problems encountered in photoionization models of the NLR. In comparison with the observations, the models predict:

A. Too weak high excitation lines. The earlier work of Stasińska (1984: ST84), who studied a large sample of optical line ratios of Seyfert 2's and LINERs, reveals that single component models fail to reproduce [Ne V]/[Ne III] (see Fig. 5 in ST84). Furthermore, even in the case of the multi-density model developed by Ferland & Osterbrock (1986: FO86), high excitation lines such as [Ne V]λ3426, C IV $\lambda\lambda$1549[1], C III]$\lambda\lambda$1909, [Fe VII]λ6087 and [Fe X]λ6375 are underpredicted by a factor of 5-15.

B. Too low electronic temperatures. The temperature (T_{OIII}) inferred from the line ratio R_{OIII} (= [O III]λ4363/[O III]λ5007) often exceeds the equilibrium temperature of models calculated with densities $n < 10^4$ cm^{-3} and solar metallicity. Typically one observes $R_{OIII} \geq 0.015$ (see ST84) while models predict significantly smaller values ($< .01$). In ST84, it is shown that the addition of a separate and much higher density component of $n \gtrsim 10^6$ cm^{-3} can reproduce the observed value of R_{OIII}. A smooth distribution of densities (as invoked by FO86[2]), however, barely reaches the low end value of $R_{OIII} = 0.015$.

C. Too small a range in He II/Hβ. ST84 found a large scatter in the ratio He II λ4686/Hβ of Seyfert 2's, which could not be explained by a universal power-law of unique index α. In

conventional ionization-bounded models, this ratio is *not* sensitive to changes in n or U (ST84; Binette, Robinson & Courvoisier 1988) but depends on the hardness of the ionizing continuum. One possibility is that α (or the temperature if a thermal source of ionizing photons is invoked) varies from object to object. Another possibility raised in ST84 was that the ionized clouds might in some cases be matter-bounded (i.e., geometrically smaller than the depth needed to absorb all ionizing photons). Viegas-Aldrovandi (1988) argued in favor of this possibility based on a weak trend for the low excitation lines to become weaker as He II/Hβ gets larger. The opposite trend would be expected if variations of the index α were invoked to explain the wide scatter of He II/Hβ.

The correlations of either critical density and/or ionization potential with the full width at half-maximum of the various lines found by Wilson (1979), Pelat et al. (1981), Filippenko & Halpern (1984), DeRobertis & Osterbrock (1984, 1986) prove that realistic models should consider a range in either or both the density n and the excitation U. This in itself does not constitute a proof, however, that all three problems raised above would be satisfactorily solved with a *smooth* distribution of densities and/or excitation.

It is our opinion that the solution to the above problems is unrelated to density stratification. Therefore, before embarking on multicomponent modelling of the unresolved NLR, it would be valuable to find a solution for the extended gas which we know is not strongly affected by collisional de-excitation.

1.2. The extended ionized regions: the ENLR or EELR

It is generally accepted that the dominant excitation mechanism of the extended gas is photoionization (see Robinson et al. 1987 and VGDP). The notion that the continuum is generated in situ (e.g. photoionizing shocks: Sutherland et al. 1993) cannot be ruled out. The cone-like structure of some ENLR suggests, however, that the nucleus is the source of the continuum (see Wilson 1995, and references therein) in at least these cases. In this situation, we can derive constraints on the geometrical dilution of the nuclear radiation reaching a given resolved patch of emission gas. If there is a distribution of cloud densities at a given location, the higher density regions would correspond to lower values of U. As the [S II] zone is in the low density limit, regions emitting more highly ionized species must have a similar or even lower densities. Let us review the evidence that models of extended gas show the same problems as they do for the NLR.

A. Too weak high excitation lines. In the ENLR of NGC1068, the [Ne V]/Hβ ratio is comparable to that found in the NLR (Evans & Dopita 1986; Bergeron et al. 1989). We find a similar situation in our own ENLR/EELR sample (Storchi-Bergmann et al. 1996: Paper I). In fact, we find a tendency for the excitation to be higher in the extended gas than in the nucleus. For the EELR of the high excitation detached cloud in PKS 2152-69, Tadhunter et al. (1988) found that that the lines of [Ne V], [Fe VII] and [Fe X] were stronger relative to Hβ than in the parent nucleus. Very high redshift radio-galaxies reveal a high excita-

---

[1]   The usage of $\lambda\lambda$ (followed by a mean wavelength in Å) means that we refer to the sum of the multiplet.

[2]   The 'mean' observed Seyfert spectrum adopted for comparison by FO86 has $R_{OIII} = 0.019$ (i.e. $T_{OIII} \sim 15\,000$ K in the low density regime).

tion UV spectrum with strong lines of C IV and C III] (Villar-Martín et al. 1996; McCarthy 1993 and references therein).

B. Too low electronic temperatures. Tadhunter et al. (1989: TRM89) pointed out the temperature problem encountered in EELR. The range observed was $0.03 \geq R_{OIII} \geq 0.01$. More detailed observations now include Cen A (Morganti et al. 1991) and 3C227 (Prieto et al. 1993). Our observations reported in Paper I were designed to extend this kind of study of R_{OIII} to the ENLR of Seyferts. Our sample, including the two radio-galaxies, indicates values in the range $0.023 \geq R_{OIII} \geq 0.011$ (i.e., $16\,000\,K \geq T_{OIII} \geq 12\,000\,K$).

C. Too low values of He II/Hβ. Tadhunter (1986) found that the He II/Hβ ratio of EELR often exceeds the value predicted by ionization-bounded[3] models with a canonical power-law (while for nuclei it was only the large width of the scatter which posed difficulty). In our sample, we find similarly high values. Such large ratios cannot be reproduced with *any* power-law index if all the clouds are ionization-bounded(e.g., Binette, Courvoisier & Robinson 1988).

1.3. Solutions which have been proposed

The presence of shock waves, providing either collisional ionization in addition to photoionization by the central source or photoionization by the shock itself would certainly impact the line ratios and might solve some or all the above problems. We refer the reader to the ongoing and extensive work carried out by Contini & Viegas-Aldrovandi (1989), Dopita & Sutherland (1995, 1996), VGDP and Sutherland et al. (1993) on this subject. Our work concerns new results with pure photoionization models, which have the merit of not requiring additional excitation mechanisms.

Outside the arena of shocks, the specific solutions which have been proposed so far usually solve only one of the above problems. For instance, the very strong high excitation lines might be the result of an absorbed and therefore very hard continuum (NLR: Ferland & Mushotzky 1982; ENLR: Evans & Dopita 1986; Bergeron et al. 1989; Nazarova 1995). The apparently high values of T_{OIII} might instead be the result of a high density component but this possibility exists only for the unresolved NLR and therefore has too narrow a range of applicability. Reducing metallicity by a factor $\gtrsim 3$ is one possibility (NLR: Ferland & Mushotzky 1982; Ferland & Netzer 1983; ENLR: TRM89) but such is unlikely to be applicable to the NLR (and ENLR?) gas, which we might reasonably expect to have solar or higher metallicity. Another possibility which increases T_{OIII} is the presence of an intense flux of relativistic electrons (see Viegas-Aldrovandi & Gruenwald 1988). However, there is no evidence that the temperature is correlated with the presence of strong radio emission. Dust grain photoionization can also raise the temperature significantly provided U is sufficiently

high (cf., Appendix C in Baldwin et al. 1991). The scatter in the nuclear He II/Hβ ratio and its extreme values outside the nucleus are best explained by invoking differing degrees of thinness in the emitting clouds (for the NLR: Viegas-Aldrovandi 1988; the EELR: Tadhunter 1986; Morganti et al. 1991; Viegas & Prieto 1992; VGDP; and the ENLR: Haniff et al. 1991).

In this work we favour a solution resembling that developed by Viegas & Prieto (1992) which we will show has the potential of resolving simultaneously all three problems. It also shares some similarities with the work of Péquignot & Dennefeld (1983) who modelled a bright filament in the Crab Nebula which presents interesting similarities to NLR spectra.

2. The particularities of matter-bounded clouds

2.1. Dichotomy of matter-bounded versus ionization-bounded clouds

Let us first review in more detail the conclusions reached from comparisons between pure photoionization models with matter-bounded (MB) clouds and observations of extended gas. On the one hand, Morganti et al. (1991) use a smooth distribution of clouds of different thicknesses, while on the other Viegas & Prieto (1992: VP92) simply combine in varying proportions very thin matter-bounded clouds with ionization-bounded clouds. Both succeed in accounting for the scatter as well as the high values of the He II/Hβ ratio in EELR. However, both papers conclude that the temperature problems cannot be solved in this manner. Our contention is that, although a 'smooth' distribution of matter-bounded clouds would not indeed produce sufficiently high T_{OIII}, a simple combination of matter-bounded and ionization-bounded clouds can simultaneously solve all three problems. VP92 did not obtain this solution because they used too thin[4] a cloud for the matter-bounded component and too low an ionization parameter (U=0.01). Such a very thin, matter-bounded component does not emit any significant [O III] (nor is it quite hot enough when U=0.01), and so combining it with ionization-bounded clouds does not raise the global R_{OIII}.

2.2. Building blocks: proportionate matter-bounded clouds

From the perspective of matter-bounded clouds, high temperatures are easy to reproduce if we select a sufficiently high ionization parameter (cf. Péquignot & Dennefeld 1983). To illustrate this, we plot in Fig. 1 the quantities T_{OIII} (panel a) and R_{OIII} (panel b) as a function of the ionization parameter U. In these calculations with the code MAPPINGS (Sect. 3.2), the slab's thickness is such that the fraction of absorbed ionizing photons is 30% at all U. This fraction of ionizing photons absorbed (hereafter F_{MB}) is a useful parameter for defining the thickness of the slab, as it also gives a measure of the fraction of the Hβ flux generated within the MB component relative to the optically thick case. The most interesting result is that a power-law with $\alpha \approx -1.3$ can indeed produce temperatures $\gg 10\,000\,K$ if U is sufficiently high. The main reason for the dependence of

---

[3] Ionization-bounded clouds are sufficiently thick to absorb essentially all the ionizing radiation.

[4] VP92 report having used a Lyman limit opacity $\tau_{\nu o}^{H} < 1$ for their matter-bounded component; in our calculations $\tau_{\nu o}^{H} > 1$.
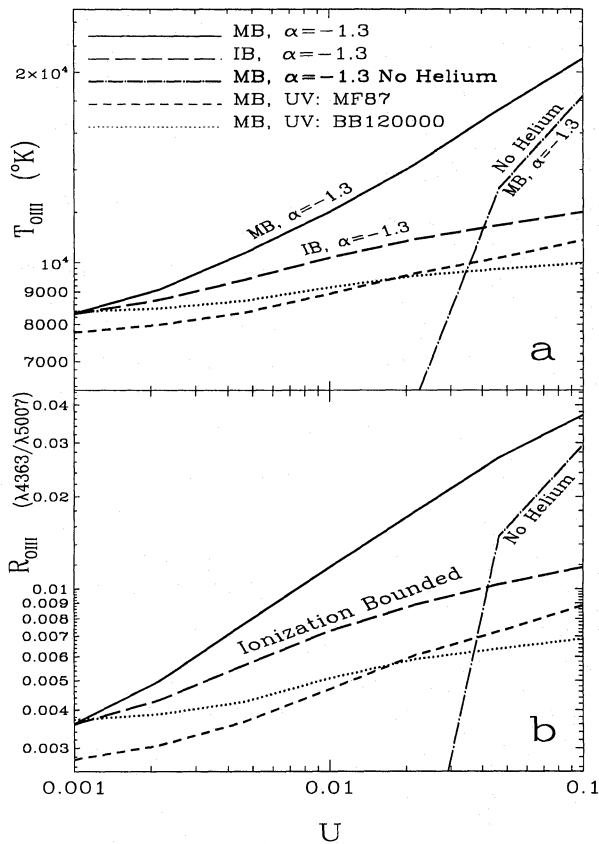
Fig. 1a and b. Sequence of matter-bounded (MB) photoionization calculations [except for the long-dash curve which is ionization-bounded (IB)] of increasing ionization parameter U. Panel **a** is a plot of the equilibrium electronic temperature inferred from the R_{OIII} ratio [plotted in panel **b**]. The ionizing continuum is a power-law except for the short dash curve (multi-segmented power-law, see Mathews & Ferland 1987) and the dotted curve (black-body of 120 000 K). All MB models are set to absorb 30% of the ionizing photons ($F_{MB}=0.3$). Abundances are solar (Z=1). The long dash-dotted curve represents a plasma without any He but still with Z=1. The curves have the same meaning on the two panels.

Fig. 2a and b. Variation of the temperature (T_e) and of the effective heating rate (Γ/n^2) as a function of depth into a slab photoionized by a power-law of index $\alpha = -1.3$. The depth is expressed in terms of the fraction, F_{MB}, of ionizing photons absorbed up to that point in the slab. The dashed curves represent the integrated column densities of O^{+2} (long dash, panel **a**) and He^{+2} (short dash, panel **b** as a function of F_{MB}. The abundances of the gas are solar and the ionization parameter is U = 0.04 (Eq. 1).

temperature on U is that most of the heating in the MB cloud is caused by photoionization of He^+. This is shown by the He free models (dash-dotted curve) which have a much lower T_{OIII} except for $U \geq 0.04$, which marks the onset of heating by photoionization of metals.

Fig. 1 also illustrates how blackbodies are relatively ineffective in generating high T_{OIII} as compared to power-laws. Such thermal energy distributions were considered by ST84 and Binette, Robinson & Courvoisier (1988) for the NLR and by Péquignot (1984) for LINERs (T_{bb} = 80 000 K). Similarly low T_{OIII} values characterize the multi-segmented distribution of Mathews & Ferland (1987), which is intended to model the big UV bump and the soft to hard X-ray spectra of AGN.

We emphasize that values of R_{OIII} in the range 0.015-0.025 are only obtained for MB clouds which truncate the O^{+2} zone. A much thicker MB slab is more luminous in [O III]λ5007 but
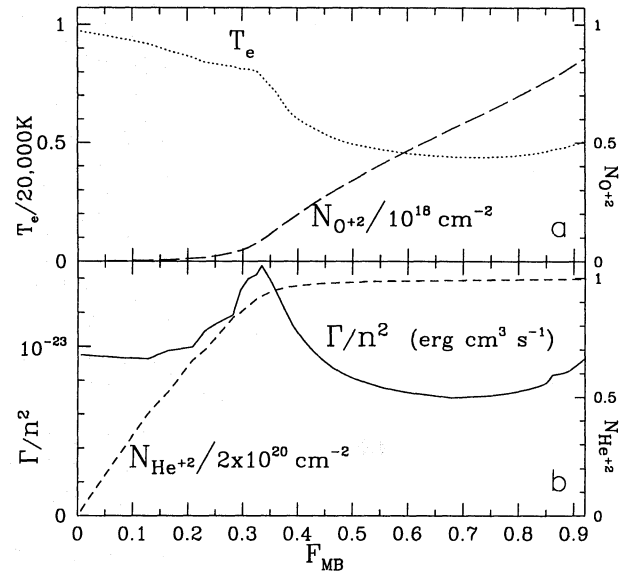
significantly colder which depresses the integrated R_{OIII} value. The ionization-bounded (IB) models of increasing U plotted in Fig. 1 (long-dash curve) illustrate well the difficulty that any optically thick model has in reaching high values of R_{OIII} (see also TRM89), even when U is high. The reason for this is that the internal temperature within the O^{+2} zone decreases with increasing depth, hence the importance of considering a sufficiently thin slab.

To illustrate this point further, let us consider the structure of a photoionized slab with U= 0.04 as shown in Fig. 2 and compare the internal temperature behaviour (panel a) with the behaviour of the O^{+2} column density, as a function of depth. It is apparent that the temperature decreases rapidly from 16 000 K to 10 000 K within the region where the O^{+2} column density reaches $\sim$ 20% of the asymptotic value. This sudden temperature decrease coincides with a decrease in the effective heating rate (solid line: Γ/n^2) at $F_{MB} \approx 0.35$ and is due to the disappearance of ionizing photons in the region 54-200 eV responsible for photoionization of He^+ (the dominant heating process as discussed above [Fig. 1]). This is confirmed in Fig. 2 by the behaviour of the He^{+2} column density (panel b) which reaches its asymptotic value not far beyond the position of the peak in the heating rate (at $F_{MB} \approx 0.35$).

We have seen that to obtain sufficiently high temperatures the MB clouds must be sufficiently thin that their temperature is governed by photoionization of He^+. On the other hand, the MB clouds must also be thick enough to contribute significantly to the [O III] lines. Finally, as will become clear later, the other

Table 1. Data sample and dereddened line ratios relative to [O III]λ5007Å (=100)

Galaxy name	Symbol	Type	r (kpc)	A_V (mag)	He II 4686	[O III] 4363	[O II] 3727	[O I] 6300	[S II] 6725	[N II] 6583	[Ne V] = 3426	Hα 6563	Hβ 4861
ESO 362-G8	*open* □	Sy 2	Nuc.	–	–	–	11.6	–	17.9	58.9	11.9	33.2	–
			3.0 NE	0.4	3.6	1.1	30.4	1.6	11.2	21.9	4.4	28.9	9.3
Mrk 573	*open* ○	Sy 2	Nuc.	0.6	3.4	1.3	18.7	2.6	13.6	21.3	9.2	25.4	8.1
			1.9 NW	0.8	3.4	1.5	39.3	2.0	15.7	21.6	8.3	28.9	9.3
			1.9 SE	2.2	3.4	2.0	51.0	1.3	12.9	16.9	24.8	26.0	8.4
NGC 526A	*open* △	Sy 1.5	Nuc.	1.8	2.7	2.1	38.8	2.3	9.8	14.1	13.8	20.7	6.7
			2.5 NW	0.04	2.4	2.3	74.0	6.7	39.0	45.7	2.1	45.4	14.6
Pks 0349-27	*filled* □	NLRG	Nuc.	–	2.3	<1.6	110	18	58.6	45.1	4.4	57.7	20.1
			13 NE	–	3.5	1.8	45.6	1.3	11.4	13.1	3.9	27.4	9.2
			13 SW	–	3.2	1.6	37.3	1.7	9.5	8.5	5.0	25.4	9.5
Pks 0634-20	*filled* △	NLRG	Nuc.	2.5	3.5	<0.8	36.8	2.4	10.0	13.8	15.9	27.0	8.7
			5.8 SE	0.4	4.4	1.9	6.8	–	2.6	5.2	18.0	26.6	8.6
			9.7 NW	0.6	6.9	1.9	3.7	–	3.2	3.8	33.5	30.5	9.8

important problem of the strength of the high excitation lines is also solved with MB clouds of sufficiently high ionization parameters (U ≳ 0.04).

3. Data sample and the modelling procedure

3.1. The sample

The models will be compared with our own observations (Paper I) which were specifically designed to measure the key *weak* lines of [O III]λ4363, He II λ4686 and [Ne V]λ3426, a difficult proposition for the lower surface brightness ENLR gas. The many internal correlations present between the different line ratios (Sect. 4) confirm that the effort was worthwhile.

The sample is presented in Table 1 and comprises Seyfert 2's and NLRG's except for NGC 526A which is a Seyfert 1.9. For each object, spectra were obtained at the location of the nucleus and – depending on the S/N – at two or one off-nuclear positions along the slit. The projected distances on the sky from the nucleus to the off-nuclear positions are listed in Column 4 assuming $H_o = 75 \, \mathrm{km \, s^{-1} Mpc^{-1}}$ and $q_0 = 0.5$. The data reduction techniques are described in detail in Paper I. The observed Balmer decrement was used to determine the reddening corrected ratios listed in Table 1 assuming an intrinsic ratio of Hα/Hβ = 3.1.

Table 1 also includes the symbol used in the figures (Column 2), the activity type (Column 3), the obscuration A_V (Column 5) and the (dereddened) line ratios [with respect to [O III]λ5007 (=100)] which are used in this paper. Note that upper limits are not shown in any diagram. The errors in the measurement of the weakest lines is estimated at ≤ 30%.

3.2. The computer code and the parameters Z, μ

The data will be compared with photoionization models which were computed using the multipurpose photoionization-shock code MAPPINGS. The latest version is described in Binette

et al. (1993a,b). We adopt the collisional excitation rates of hydrogen calculated by Aggarwal et al. (1991).

As for gas metallicity, we scale with a factor Z the solar abundance set of trace elements compiled by Anders & Grevesse (1989). He/H is kept constant at 0.1. Unless specified otherwise, we consider the solar case with Z=1.

Dust is considered to be mixed with the ionized gas, and the code includes heating by dust photoionization. The dust content of the photoionized plasma is described by the quantity μ which is the dust-to-gas ratio of the plasma expressed in units of the solar neighborhood dust-to-gas ratio. We adopt the extinction curve produced by a distribution of very small grains of silicate and graphite with sizes in the range $0.005 \leq a \leq 0.03 \mu$m. The population density of grains is assumed to vary as $a^{-3.5}$ where a is the grain size. The extinction curve was computed by Martin (cf., Magris et al. 1993) and extends from infra-red to X-rays.

The calculations in this work use a constant dust-to-gas ratio of $\mu = 0.015$ which has a negligible effect on line transfer and on the gas heating. After exploring models with higher μ, we found that the effects of dust were of secondary importance in our study of matter-bounded models and would unduly complicate the exploratory nature of the present work. We will, therefore, comment only briefly on the results of using higher values of μ. Depletion of the gas phase metals (very minor at $\mu = 0.015$) was taken into account following the prescription given in Appendix A of Binette et al. (1993b). At metallicities other than solar, μ=0.015 Z.

3.3. The physical distinction between matter- and ionization-bounded clouds

We hereafter propose a new approach to the interpretation of the observed variations in the degree of excitation of the line spectra of AGN. These variations are traditionally interpreted as resulting from variations of the ionization parameter. We investigate in this paper the possibility that the apparent varia-
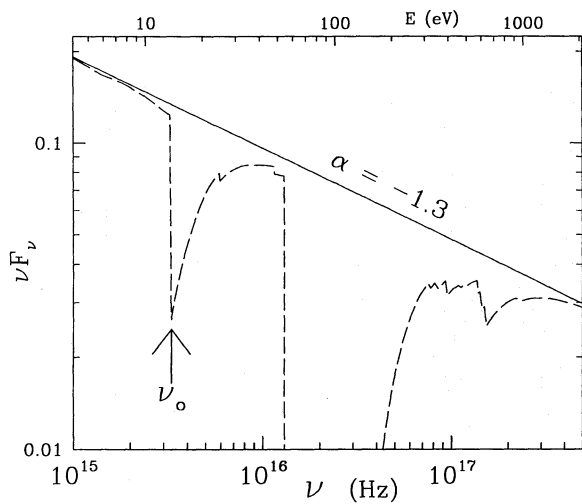
Fig. 3. The flux density of the power law incident on the matter-bounded slab is plotted as $\nu F\nu$ (solid line). The long dashed curve represents the ionizing energy distribution escaping the back of a matter-bounded slab which is sufficiently thick to absorb 40% of the ionizing photons. The abundances of the slab are solar and the ionization parameter is $U_{MB} = 0.04$. This modified energy distribution is used as the ionizing spectrum for the ionization-bounded clouds.

Fig. 4a and b. Cartoons of two possible geometrical distributions of matter-bounded (MB) and ionization bounded (IB) components. The luminosity of any component is essentially governed by the solid angle it covers at the central UV source. The inner clouds (NLR) are denser and smaller than those at larger radii, where the cloud sizes become sufficiently large that individual components become resolvable (ENLR or EELR). In our models, the IB clouds are of lower excitation mostly because they see an ionizing continuum filtered by the MB component. **a** The MB clouds are closer to the ionizing source and shadow the more distant IB clouds which see a more dilute radiation field and hence have lower U. Supposing a planar or cylindrical distribution of obscuring material, the relative numbers of *visible* IB and MB clouds can vary considerably according to the perspective of the observer. **b** The IB component is associated with the dense core (higher pressure) of a gas cloud surrounded by a tenuous matter-bounded evaporating halo.

tions in excitation represent instead different proportions of two different populations of line emitting clouds. The first population is 'matter-bounded' (MB) clouds, the spectrum of which is found given by photoionization calculations truncated after a fraction F_{MB} of impinging ionizing photons has been absorbed. The excitation degree of this MB component is very high. The second population is 'ionization-bounded' (IB) clouds, which are much more opaque to the ionizing radiation (absorbing a fraction $F_{IB} \simeq 1$ of impinging photons) and of much lower excitation. We adopt $F_{MB} = 0.40$ and $F_{IB} = 0.97$ in the calculations presented here, the justification of which is given below.

An original aspect of the current approach is that we assume the IB clouds are photoionized only by the UV photons which have leaked through the MB clouds. Thus the input ionizing spectrum reaching the IB clouds has been partially absorbed (filtered) by the MB clouds. Fig. 3 illustrates the energy distribution available to the IB component (dashed line).

The approach taken adopts the view that an unaltered power-law would always generate a population of very high excitation matter-bounded clouds, as we now discuss. The force which couples the MB cloud structure to the radiation field would presumably be radiation pressure. One might imagine, for instance, that the MB gas corresponds to a thin halo surrounding a dense cloud core. The intense radiation impinging on the outer layers of the cloud would accelerate these outer layers away, leading to a gradual photoevaporation of the cloud (cf. Bertoldi 1989; Bertoldi & McKee 1990). The existence of a matter-bounded characteristic thickness in the range $F_{MB} \simeq 0.35 - 0.40$ might result from the peak in the heating rate (solid line, Fig. 2b) which we tentatively interpret as a stalling point in the accelerative outflow of thin MB gas layers. As the gas accelerates away from the
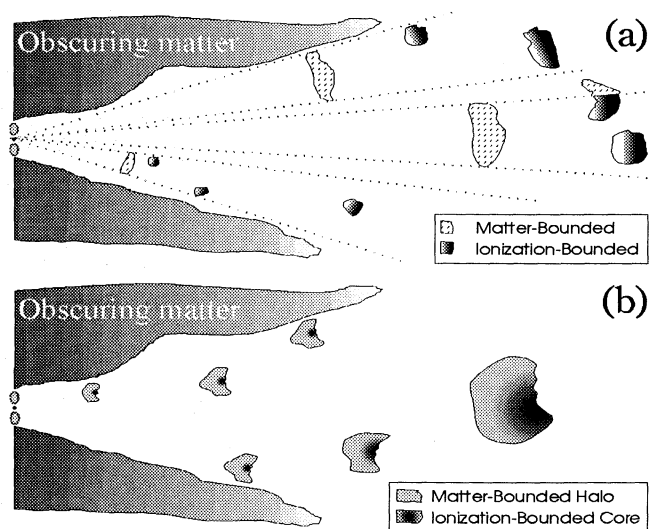
core due to radiative pressure and gets less dense and thinner, it also gets hotter, which drives the expansion process further. In this picture, the IB component corresponds to the dense core of the cloud.

The ionizing radiation available to the IB component has leaked through the MB clouds and is quite different from the original power-law. It consists mostly of hard photons (dashed line in Fig. 2) which interact much less effectively with the gas since their energy is well above either the He^+ or the H^0 ionization thresholds. This suggests there is little coupling between the gas density of the IB component and the hard radiation, with the IB gas condensations simply passively absorbing the latter. Unlike the matter-bounded clouds, which all share the same excitation as a result of their coupling to the radiation field, the IB clouds might, therefore, not be characterized by a unique excitation or value of U_{IB}. In this paper we have explored a single value of U_{IB} in order to keep the modelling procedure as simple as possible.

3.4. A geometrical representation of the clouds' space distribution

Depending on the ratio of the spatial resolution to the dimensions of the gaseous condensations, we can distinguish two situations. In the unresolved case, which applies to the NLR of Seyferts, we obtain a statistical and undifferentiated combination of the two populations of clouds leading to the 'mean' NLR Seyfert spectrum. In the case of radio-galaxies, where we have much larger scale gaseous components, we expect a dichotomy between high excitation and low excitation condensations, as is generally observed for EELR (Fosbury 1989), and which we here associate with partially resolved MB and IB clouds, respectively.

We present in Fig. 4 schematic diagrams illustrating two possible distributions of MB and IB clouds. In our scheme, the Hβ luminosity of any cloud is essentially governed by the solid angle it occupies within the opening angle of the ionizing cone. The inner clouds (NLR) are envisaged to be both dense and small and below our resolution. As is apparent in the diagram 4a, the observer's perspective is bound to play an important role in the observed excitation of the ionized gas. For example, if we suppose that obscuring material hides part of the NLR, as proposed for some Seyfert 2 galaxies (e.g., NGC 1068; Cameron et al. 1993), then the relative prominence of the two emission-line components would depend on the angle from which we look at the nuclear region. The IB component would dominate the high excitation MB component if, for instance, most MB clouds in Fig. 4a were hidden by obscuration. The converse would be true if our view of the NLR is dominated by the unresolved denser, inner MB clouds, with the more diffuse IB clouds further out in the disk of the galaxy (i.e. outside the NLR).

A complementary interpretation of the IB/MB dichotomy is that the IB component corresponds to the denser core of a diffuse matter-bounded halo as depicted in Fig. 4b and discussed in the last subsection. Alternatively, the IB clouds are not necessarily back to back with the MB clouds but at some distance behind them, as depicted in Fig. 4a. Our treatment of the radiative transfer is more consistent with the second possibility (although the two possibilities are not mutually exclusive), since we opted to neglect the contribution of the diffuse field from the MB clouds to the ionization of the 'detached' ionization-bounded clouds. The rationale behind this assumption is that the diffuse field emitted by the MB clouds is isotropic while the ionizing continuum is radial. In any event, this neglect of the diffuse field 'external' to the IB clouds does not alter significantly their emission line spectra.

3.5. On defining the ionization parameter and/or pressure of the two components

The input ionization parameter is defined as the quotient of the density of impinging ionizing photons and the outer density of the gas cloud:

$$U = \frac{\int_{\nu_o}^{\infty} \phi_\nu \, d\nu / h\nu}{c \, n} = \frac{\phi_H}{c \, n} \qquad (1)$$

where ϕ_ν is the monochromatic ionizing energy flux impinging on the cloud, ν_o the ionization potential of H, n the total gas density in the front layer of the slab and c the speed of the light.

In choosing the input spectrum of ionizing radiation, we opted to find the closest index to the canonical values proposed in the literature (i.e., $\alpha = -1.4$ or -1.5; e.g., FO86) and yet still produce high enough R_{OIII}. We therefore adopt $\alpha = -1.3$ since steeper power-laws produce too low a temperature[5]. Flatter power-laws can, in principle, be used although in this case the ionization-bounded clouds must become *more* matter-bounded ($F_{IB} \approx 0.90$) to avoid excessive fluxes in the low excitation lines.

The only ionization parameter which we determine a priori is that of the MB clouds which see the unaltered ionizing distribution, ϕ_ν. We adopt $U_{MB} = 0.04$ which allows us to reach the high electronic temperatures of $T_{OIII} = 15\,000$ K ($R_{OIII} = 0.02$) representative of the extranuclear regions. We emphasize that U_{MB} is not as critical to the line ratios as in the standard single zone ionization-bounded model. Higher U_{MB} values (at constant He II/Hβ) will result mostly in higher intensities of highly ionized species (e.g. [Fe X]λ6375, C IV, [Fe VII]λ6087, [Ne V]).

As is customary in interpretation of extended emission regions, we adopt the low density regime and for concreteness fix the density at $n_{MB} = 50$ cm^{-3}. This gives us a *total* gas pressure for the front layer of $P_{MB} = 2.1 \, 10^6$ K cm^{-3}. We adopt the isobaric prescription, that is the calculations demand the gas pressure be constant within any MB (of pressure P_{MB}) or IB (of pressure P_{IB}) clouds, with the behaviour of the total density as a function of distance into the cloud ($n(x)$) modulated by the behaviour of the temperature and by the ionization fraction of the gas.

Rather than specifying directly the ionization parameter of the IB clouds (which, we emphasize, see a different continuum), we independently fix their pressures. In order to avoid having the total (MB+IB) [O III]λ5007/Hβ ratio much too large, it is easily shown that the IB clouds must contribute less [O III]λ5007 flux than the MB component. This is realized using either a greater density[6] for the IB clouds (supposing they are close to or represent the cores of the MB clouds) or some additional geometrical dilution of the modified continuum they see. By trial and error, we find that $P_{IB} \sim 20 P_{MB}$ (which results in $U_{IB} = 5.2 \, 10^{-4}$) gives a very acceptable fit of the summed spectrum (IB+MB) to the observed range of line ratios in our sample. In the low density regime in which the line spectrum does *not* depend on ϕ_H or n separately, but on their ratio (U), we can consider the following two interpretations of this pressure jump as totally equivalent. Either the IB clouds have a greater density ($n_{IB} \approx 20 n_{MB}^{bck}$, where n_{MB}^{bck} is the density at the back of the MB slab[7]) or the fil-

---

[5]   If we increase the dust content of the MB component to μ_{MB}=0.15, a power law with α=-1.4 gives similar results to those presented here with μ=0.015 and α =-1.3.

[6]   The decrease in [O III]λ5007 luminosity achieved with higher P_{IB} is *not* caused by collisional deexcitation but is simply the result of a reduction in U when a higher density (i.e., pressure) is used (see Eq. 1).

[7]   Given the isobaric prescription, the density at the back is higher than at the front because of the temperature gradient.

tered continuum is diluted by a factor $1/20$ as a result of the IB clouds being a factor of $\sqrt{20}$ more distant than the MB clouds from the ionizing source. Since in the calculations presented in Sect. 4, we have explicitly used the pressure jump prescription (i.e. $n_{IB} = P_{IB}/(2.1\,kT) = 2\,300\,\mathrm{cm}^{-3}$) rather than diluting the radiation, it should be kept in mind that collisional deexcitation has somewhat reduced our [O II] and [S II] line intensities.

The above procedure defining the MB and IB components can be summarized as follows. Once the continuum distribution is adopted, and assuming for definiteness solar metallicity, we select a single ionization parameter for the MB component which produces high enough T_{OIII}. The MB clouds should be sufficiently thick to include a fraction of the O^{+2} zone in order that the MB component dominates in the line of [O III]$\lambda 4363$. It should be sufficiently thin, however, to ensure a high enough T_{OIII}. We have seen that this occurs at a depth near the maximum in the heating rate (Γ/n^2: Fig. 2b). In the case of a power-law of $\alpha = -1.3$ and with $U_{MB}=0.04$, these considerations guide us to a value of $F_{MB}=0.40$, which results in He II/H$\beta = 0.87$ from the MB component alone. From these calculations, we determine the spectral energy distribution exiting the matter-bounded clouds (dashed line in Fig. 3) and use it as the input continuum to the IB clouds. The calculations of the IB clouds proceed by taking into account their own internal pressure, which we set to $20P_{MB}$. To avoid excessive fluxes in the low excitation lines, the ionization-bounded clouds are truncated at $F_{MB}=0.97$. The MB and IB emission line spectra (cf. Table 2) can be combined together with varying relative weights. The Hβ luminosities per unit area per unit density are $6.74\,10^{-5}\,n_{MB}\,\mathrm{erg\,cm\,s}^{-1}$ and $1.18\,10^{-4}\,n_{MB}\,\mathrm{erg\,cm\,s}^{-1}$ for the MB and IB components, respectively, assuming the same geometrical dilution of the incident radiation for both components.

3.6. $A_{M/I}$: a new excitation sequence of models

The originality of the above procedure lies in the fact that we no longer account for variations in excitation between AGN, or between different positions in the EELR, by a change of the ionization parameter, but rather by differing ratios of two distinct populations of photoionized clouds. By fixing the thickness of each gaseous component (F_{MB}, F_{IB}), we predetermine their reprocessing efficiency. Their luminosity in Hβ is then solely governed by the solid angle each component subtends at the ionizing source. Let us define $A_{M/I}$ as the parameter representing the ratio of the solid angle subtended by the MB clouds to the solid angle subtended by the IB clouds, where, of course, only those clouds visible to the observer are included (cf. Fig. 4a). Any line ratio R^i_{seq} of line i relative to Hβ for a given model of the $A_{M/I}$-sequence is found by combining the MB and IB ratios of Table 2 in the following manner:

$$R^i_{seq}(A_{M/I}) = \frac{R^i_{IB} + 0.568 A_{M/I} R^i_{MB}}{1 + 0.568 A_{M/I}} \tag{2}$$

where 0.568 represents the ratio of the luminosity of Hβ from the MB component to that of the IB component. A larger value of $A_{M/I}$ implies a larger weight given to the MB component and,

Table 2. MB and IB line ratios relative to Hβ (=1.0)[a]

i	λ (Å)	R^i_{MB}	R^i_{IB}
C IV	1549[b]	12.6	$3.9\,10^{-3}$
He II	1640	7.05	$4.3\,10^{-2}$
O III]	1663[b]	0.78	$1.3\,10^{-2}$
N III]	1749[b]	0.25	$6.6\,10^{-3}$
C III]	1909[b]	4.26	0.37
C II]	2326	$1.9\,10^{-2}$	0.48
[Ne IV]	2423[b]	1.59	$1.2\,10^{-3}$
Mg II	2800	$5.5\,10^{-2}$	3.60
[Ne V]	3426	2.96	$4.7\,10^{-4}$
[O II]	3727[b]	0.10	7.77
[Ne III]	3869	0.88	0.70
[S II]	4072[b]	$5.2\,10^{-5}$	0.19
[O III]	4363	0.33	$1.6\,10^{-2}$
He II	4686	0.87	$7.7\,10^{-3}$
[O III]	5007	16.9	3.67
[N I]	5200[b]	$2.7\,10^{-5}$	0.15
[N II]	5755	$3.4\,10^{-4}$	$5.0\,10^{-2}$
He I	5876	$2.9\,10^{-2}$	0.16
[O I]	6300	$1.4\,10^{-4}$	0.76
Hα	6563	2.78	2.89
[N II]	6583	$1.0\,10^{-2}$	3.82
[S II]	6724[b]	$5.5\,10^{-4}$	1.76
[Ar III]	7135	$6.4\,10^{-3}$	0.33
[Ca II]	7291[c]	$9.3\,10^{-3}$	0.62
[O II]	7330[b]	$1.5\,10^{-3}$	0.14
[S III]	9531	$2.4\,10^{-2}$	2.58

[a] Ionizing continuum of index $\alpha = -1.3$
[b] Sum of doublet terms
[c] Ca/H is depleted by 0.46 dex, see Sect. 3.2

therefore, a *higher* excitation spectrum. The column densities of *ionized* hydrogen for the two components are

$$N^{H^+}_{MB} \approx 10^{23}\,U_{MB}F_{MB}\,\mathrm{cm}^{-2} \tag{3}$$

$$N^{H^+}_{IB} \approx 10^{23}\,U_{MB}(1 - F_{MB})F_{IB}\frac{P_{MB}}{P_{IB}}\,\mathrm{cm}^{-2} \tag{4}$$

Strictly speaking, $A_{M/I}$ cannot be lower than unity since by definition the MB clouds are intervening clouds between the nuclear ionizing source and the IB clouds (see Fig. 4). However, in the current popular schemes of AGN unification, perspective can play an important role due to obscuration of the inner regions (by large molecular clouds or by a dusty disk). It is then reasonable to postulate that in Seyfert 2's and NLRG's only a small fraction of all the MB clouds (expected to lie somewhere inbetween the continuum source and the IB clouds) are directly visible to the observer, thereby giving physical meaning to an 'apparent' $A_{M/I} < 1$ for a distant observer. The schematic diagram of Fig. 4a illustrates how the observer's angle of view could affect the relative number of IB versus MB clouds and therefore introduce changes in the line ratios corresponding to the change in $A_{M/I}$.

Amongst the different possibilities for defining the IB clouds, one might consider a different case in which the IB clouds see the ionizing source directly instead of an absorbed continuum. However, we consider our approach more promising for the following reasons:

1. The IB clouds are characterized by a low He II/Hβ ratio and so objects with weak He II can now be accounted for in a natural way by supposing $A_{M/I}$ is lower than unity. On the other hand, conventional models are inconsistent with both extremes of He II/Hβ for a canonical power-law of $\alpha \simeq -1.4$ or flatter.

2. Since we obtain our sequence as a function of $A_{M/I}$ by combining two distinct populations of clouds with very different emission spectra, something physical must distinguish them. In the adopted procedure, the two components are physically different because the ionizing continuum is different. We have proposed that the truncation of the MB clouds coincides with the exhaustion of the He$^+$ ionizing photons and that the IB clouds are of lower excitation due to the much lower radiation pressure exerted by the filtered continuum.

4. Comparison of the $A_{M/I}$-sequence with observations

In the following figures, we compare the observed line ratios of our sample of extended EELR and ENLR regions, including their respective nuclear spectra, with the new $A_{M/I}$ photoionization sequence as well as with the conventional U sequence. In Figs. 5-10 and 12-13, filled symbols correspond to radio galaxies and the open symbols to Seyferts (see legend in Table 1). A dotted line connects measurements at different locations in the same object (e.g., Fig. 5).

In order to visually distinguish the extended gas from the NLR of the same galaxy, we use a larger symbol for the unresolved nuclear ratios. The NLR presumably consists of clouds with a wide range in densities (possibly ranging as high as 10^6 cm^{-3}; DeRobertis & Osterbrock 1984, 1986) and, therefore, the low density regime assumed for the extranuclear gas is not consistent with the physical conditions of the unresolved inner NLR. Curiously, this problem does not seem to affect the observed correlations, however.

4.1. The traditional excitation diagrams

A strong case in favour of photoionization as the excitation mechanism for the extended ionized gas as well as for the NLR and LINERs (Ferland & Netzer 1983) and/or cooling flows is that the emission line spectra follow well-defined trends in excitation. This was shown by Robinson et al. (1987: RBFT) who used [O I]/[O III] (6300Å/5007Å) as the excitation indicator. Such trends can be reproduced in photoionization calculations by simply varying the ionization parameter. We plot in Fig. 5 our own data adopting the diagram corresponding to Fig. 1a in RBFT. In calculating the ionization parameter sequence (long-dash line), we employed the same low density regime ($n=50$ cm^{-3}), metallicity (Z=1), energy distribution ($\alpha=-1.3$)
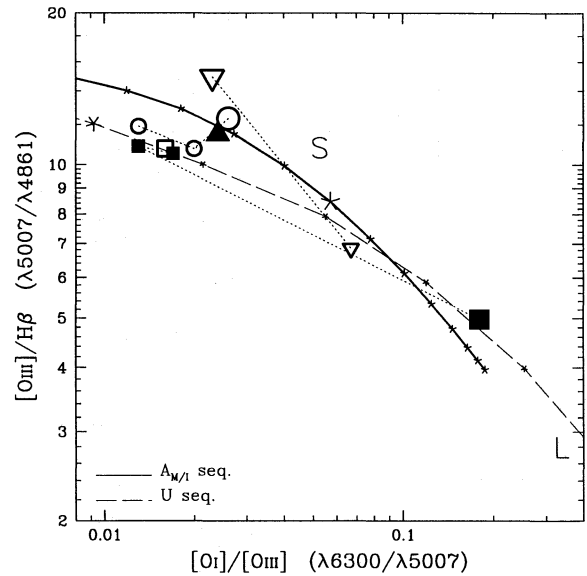

Fig. 5. Diagram of the line ratios [O III]/Hβ against [O I]/[O III]. Larger symbols denote the nuclear values. A dotted line joins measurements at different locations in the same galaxy. Filled symbols denote radio galaxies. The letters 'S' and 'L' indicate the positions of the "mean" Seyfert (as defined by FO86) and a typical LINER, NGC 1167 (Ho et al. 1993), respectively. The solid line represents the $A_{M/I}$ sequence ($0.04 \leq A_{M/I} \leq 16$) with $A_{M/I}$ *decreasing* from left to right along the solid line. The asterisks are separated by 0.2 dex in $A_{M/I}$ and the larger asterisk denotes the position of the model with $A_{M/I}=1$. The long dashed line represents the traditional U-sequence with a separation in U of 0.2 dex between models (shown as asterisks). The range covers $4\,10^{-4} \leq U \leq 10^{-1}$ (it extends beyond this figure's limits). The larger asterisk denotes the model with U = 0.004.

and opacity ($F_{Useq}=0.97=F_{IB}$) as in the $A_{M/I}$-sequence (solid line) defined in Sect. 3.

The main result of this comparison is that the $A_{M/I}$- and U-sequences are very similar and therefore equally successful in reproducing the observed trends. The interpretations implied by these two sequences are completely different, however. The U-sequence is a genuine sequence in excitation with the [O III] emitting zone becoming progressively more important relative to the [O I] emitting region as U increases, while the $A_{M/I}$-sequence produces a similar, but only *apparent*, excitation trend as a result of the high excitation matter-bounded clouds becoming more and more dominant (in number or solid angle) over the IB clouds as $A_{M/I}$ increases. The two sequences are close to each other in other excitation diagrams, such as that of Baldwin et al. (1991: BPT) shown in Fig. 6. The two sequences also occupy quite similar loci in the classification diagrams of Veilleux & Osterbrock (1987). In traditional diagrams, in which trends are acceptably fitted by varying U, the data appear to be equally well fitted by the $A_{M/I}$-sequence. We will now present new diagrams in which the two sequences present a markedly different behaviour.
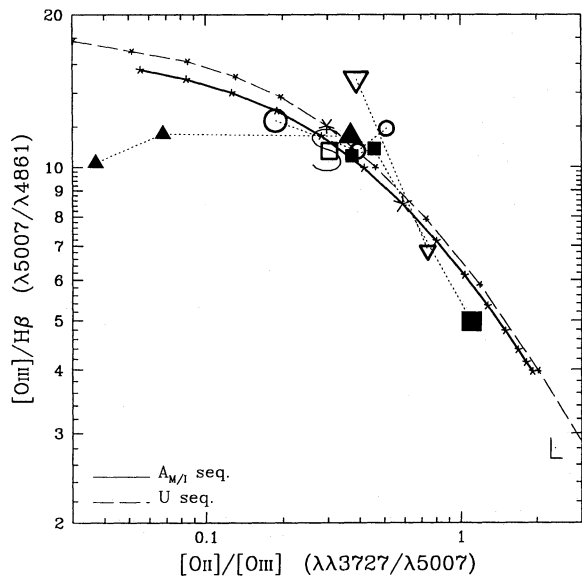
Fig. 6. Diagram of the line ratios [O III]/Hβ against [O II]/[O III] as in Baldwin et al. (1981). The symbols and lines have the same meaning as in Fig. 5.

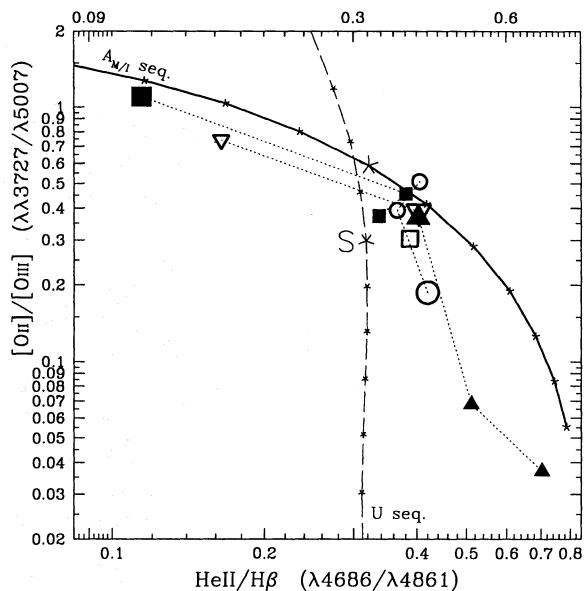**Fig. 7.** Diagram of the line ratios [O II]/[O III] against He II/Hβ. The symbols have the same meaning as in Fig. 5. The parameter $A_{M/I}$ *increases* from left to right along the solid line.

4.2. A new excitation axis: He II/Hβ

Since our starting point in adopting a MB component was to address the problem of the dispersion of He II/Hβ in AGN, we can expect the U and $A_{M/I}$-sequences to behave very differently in diagrams involving He II/Hβ. In Fig. 7, we plot [O II]/[O III] (3727Å/5007Å), the excitation axis of the first BPT diagram, against He II/Hβ. One striking result of the observations is that there exist strong correlations between He II/Hβ and the excitation of the spectrum. Such correlations have not been noticed previously in spectra of low to intermediate density regions in AGN.

The correlation of the He II/Hβ ratio with excitation is even more striking when we use the line reddening insensitive ratio [O II]/[Ne V], which extends over 2.5 dex, as shown in Fig. 8.

Another reddening insensitive line ratio, [S II]/Hα, is also found to be correlated[8] with He II/Hβ (Fig. 9). We recall that either sequence is marginally optically thick ($F_{IB}=F_{Useq}=0.97$). The intensities of the very low excitation lines, such as [O I], [S II], [N I]$\lambda\lambda$5200, depend sensitively on how thick we make the partially ionized zone which absorbs the penetrating soft X-rays. The fully thick case with $F_{IB}=1.0$ predicts too high a value of the [S II]/Hα ratio, as shown by the $F_{IB}=1.0$ sequence represented by a short dash-dotted line in Fig. 9. This discrepancy might be explained by a molecular phase (not considered by MAPPINGS) which would reduce the temperature of this zone and therefore reduce the strengths of the above forbidden lines. Alternatively, the IB cloud may consist of a very thick and dense cold core of smaller cross section than its warm thiner outer halo which would still be sufficiently thick to reprocess over 90% of

---

[8] Hints of a similar correlation appear present in the Fig. 6 of Morganti et al. (1991).

the radiation. It has often been argued before (e.g. Ferland & Mushotzky 1982; Ferland & Netzer 1983; VP92) that the the cloud's geometrical size must be truncated in order to reproduce the intensities of the [S II] and [O I] lines. It is interesting to note that the total H column density of the IB clouds implied by the fully thick case ($5.7\,10^{20}$ cm^{-2}) is 9 times higher than in the marginally thick case (solid line) in which 3% of the photons leak out. This indicates at least that the cloud sizes do not need to be fine tuned in our model.

The $A_{M/I}$ and U-sequences clearly present a very different behaviour in Figs. 7-9. We see that the U-sequences follow nearly vertical lines in these figures and are clearly totally inconsistent with our data. The $A_{M/I}$-sequence, on the other hand, accounts in a natural way for all the trends observed in these figures in which He II/Hβ is used as an axis. Not only does the new sequence solve the He II problem, but it also maintains an acceptable fit to the optical forbidden lines. We therefore continue to use the He II/Hβ ratio in our plots, since it is a very effective discriminant between the $A_{M/I}$- and U-sequences.

4.3. The high excitation lines

The weakness of the very high excitation lines is another major problem of standard models, as discussed in Sect. 1. Since our adopted U_{MB} is relatively high, we expect stronger, very high excitation lines. This is confirmed in Fig. 10 which is a plot of [Ne V]/Hβ versus He II/Hβ. The $A_{M/I}$-sequence predicts ratios which fall within a factor of three of the observed values. Furthermore, the $A_{M/I}$ values inferred from the data points in this diagram are generally consistent with the values inferred in Figs. 5-9. This is not the case for the U-sequence. If, for instance, we select an ionization parameter which fits most of the optical
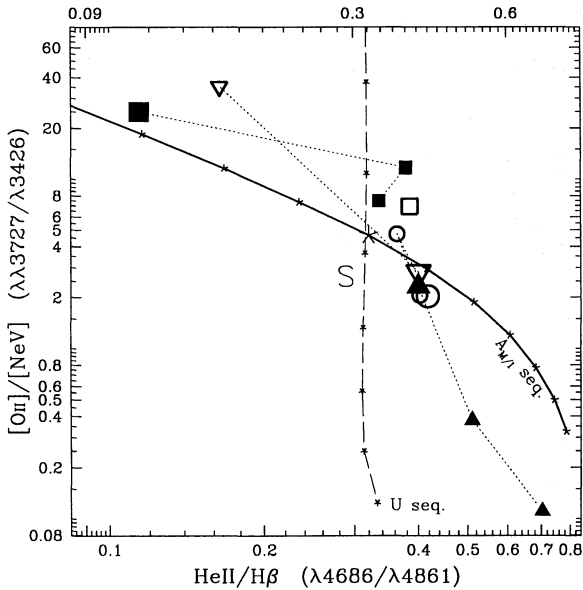
Fig. 8. Diagram of the line ratios [O II]/[Ne V] against He II/Hβ. The symbols have the same meaning as in Fig. 5. The parameter $A_{M/I}$ *increases* from left to right along the solid line. The U=0.004 model of the traditional U sequence has [O II]/[Ne V]=153, which is offscale.
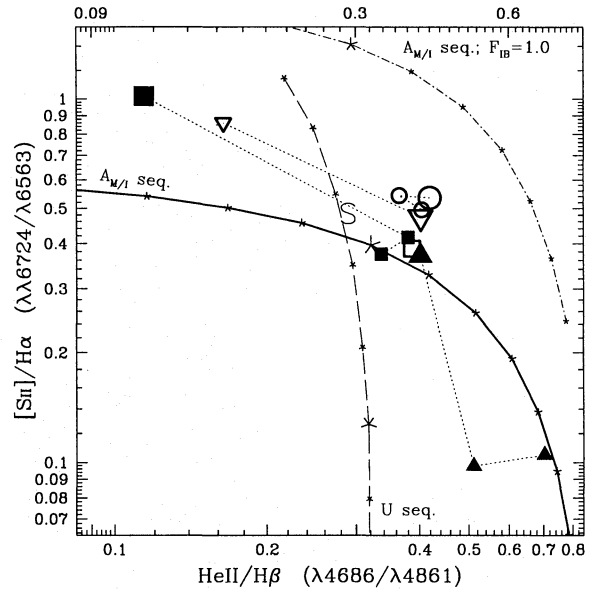
Fig. 9. Diagram of the line ratios [S II]/Hα against He II/Hβ. The symbols have the same meaning as in Fig. 5. The short dash-dotted line corresponds to an $A_{M/I}$-sequence with F_{IB}= 1.0.

lines reasonably well (i.e. U=0.004 which gives [O III]/Hβ $\simeq$ 12), we obtain [Ne V]/Hβ=0.02 and [O II]/[Ne V]=153, which are offscale in Figs. 10 and 8, respectively. Only very high U values ($\gtrsim$ 0.015) can provide an acceptable value of [Ne V]/Hβ but at the expense of the low-to-intermediate excitation lines becoming inconsistent with the data.

C IV $\lambda\lambda$1549 is another high excitation line whose intensity is poorly predicted by the standard photoionization models. As our data do not include C IV, we compare in Fig. 11 the predictions of the $A_{M/I}$-sequence with the 'mean' NLR Seyfert spectrum of FO86. Considering that in previous diagrams the spectrum 'S' falls close to models with $A_{M/I}$=1, we find that the corresponding model in Fig. 11 falls short by only a factor 2, while the traditional U-sequence underpredicts C IV/Hβ by a factor > 100 (for U = 0.004). It should be noted that the calculated C IV/C III] ratio at $A_{M/I}$=1 matches very well the value of $\sim$ 2.5 observed in many very high redshift radio galaxies (Villar-Martín et al. 1996). We therefore conclude that the observed intensities of the high excitation lines are generally reproduced by the $A_{M/I}$-sequence of models. Our code does not include Fe and we cannot, therefore, test quantitatively the agreement with the NLR [Fe X] and [Fe VII] lines. Since Fe^{+5} and Fe^{+6}, however, have similar ionization potentials to Ne^{+3} and Ne^{+4}, respectively, we can reasonably expect an improvement of the predicted strength of [Fe VII]λ6087 similar to that obtained for [Ne V]λ3426 in the $A_{M/I}$-sequence in comparison with the U-sequence.

4.4. The temperature diagram R_{OIII}

Although photoionization models were recognized by RBFT as being generally successful in explaining the observed trends in the line ratios of EELR, TRM89 discovered how inadequate such models were in reproducing the high temperatures observed. One solution discussed by these authors was to assume very low metallicities ($Z < 0.5$) for the extended gas. They indicated that a hardened spectrum would also be required to maintain an acceptable fit to the other optical lines. The solution of simply truncating the ionized clouds was discussed but not retained since it would make the [N II], [O II], [O I] lines much too weak. Morganti et al. (1991) attempted to account for the large observed values of He II/Hβ in terms of a smooth distribution of clouds of different thicknesses, but their model did not increase R_{OIII} sufficiently. As mentioned before, VP92 considered a dual distribution of MB and IB clouds but with the MB component being much too thin. We modified this scheme by using a thicker and much hotter MB component, as discussed in Sect. 2. In Fig. 12, we plot R_{OIII} against our excitation axis He II/Hβ. We see that the $A_{M/I}$-sequence (of solar metallicity gas) successfully crosses the zone occupied by the observations. Unfortunately, only upper limits could be determined for the nuclear R_{OIII} values of the radio galaxies. The moderate slope of the solid line is the result of the non-negligible [O III]λ5007 line contribution from the IB component. This slope decreases (increases) if a higher (lower) P_{IB}/P_{MB} ratio is adopted. This is shown by the dotted line in Fig. 12 which is an $A_{M/I}$- sequence calculated with a larger pressure jump (P_{IB}/P_{MB} = 40) and a harder continuum ($\alpha = -1.1$).

It should be noted that there does not appear to be any correlation between He II/Hβ and temperature. The dispersion in
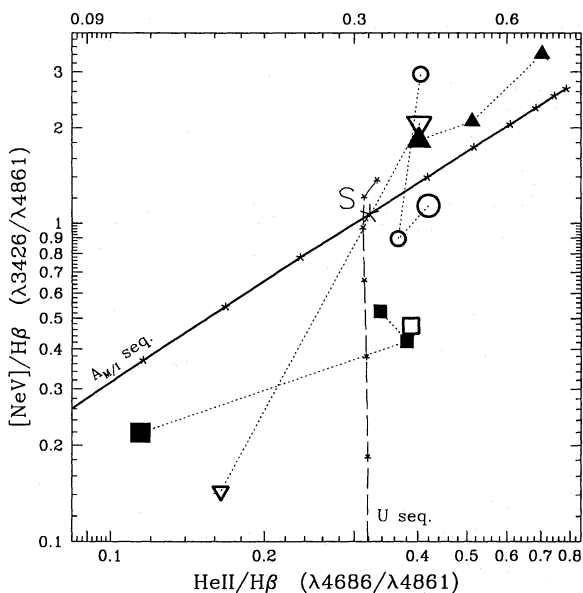
Fig. 10. Diagram of the line ratios [Ne v]/Hβ against He ii/Hβ. The symbols have the same meaning as in Fig. 5. The U=0.004 model of the traditional U sequence has [Ne v]/Hβ=0.02, which is offscale.

Fig. 11. Diagram of the line ratios C iv/Hβ against C iv/C iii]. The symbols have the same meaning as in Fig. 5. A$_{M/I}$ is *increasing* from left to right.

T_{OIII} exceeds our errors ($\leq 30\%$) and possibly points to real differences in metallicity between objects or between slit positions. Alternatively, there could be an intrinsic spread in the hardness of AGN ionizing continua. To show the effect of variation of the metallicity, we plot in Fig. 12 two sequences in Z (from 0.2 to 2 times solar) for values of A$_{M/I}$ of 0.4 and 4.0. We emphasize that the position of the A$_{M/I}$-sequence depends sensitively on the hardness of the ionizing continuum. Harder continua would raise the solar metallicity sequence in Fig. 12 (see dotted line in Fig. 12 which represents models with an ionizing continuum of index $\alpha = -1.1$) and *higher* metallicities would then be needed to agree with the data. The zero point, therefore, of a possible R_{OIII} versus Z relation is not unique and cannot be determined at this stage.

It is interesting to note that Prieto et al. (1993) report much larger R_{OIII} measurements than us at various extranuclear positions in 3C227, many ranging between 0.04 and 0.1. The error quoted of $\leq 50\%$ for the weaker lines is higher than ours. Also the spectral resolution used (≥ 11.2Å) was worse than ours (8Å) which casts some doubts on the reliability of the deblending of [O iii]λ4363 from Hγ λ4340 in regions of low surface brightness. Morganti et al. (1991) measured line intensities at many positions in the outer filaments of Cen A. The range they find for R_{OIII} is fully consistent with ours, to within the errors quoted ($\leq 40\%$). In any event, if such high values as reported by Prieto et al. (1993) were confirmed, we would need to adopt a much harder ionizing source in our models. Furthermore, we do not expect pure photoionization models to provide values of R_{OIII} in excess of 0.06. Hybrid shock-photoionization models would appear necessary if higher values are confirmed. The problem, however, with this suggestion is that it is hard to obtain [O iii]/Hβ ≥ 10 with shocks except unless photoionization by

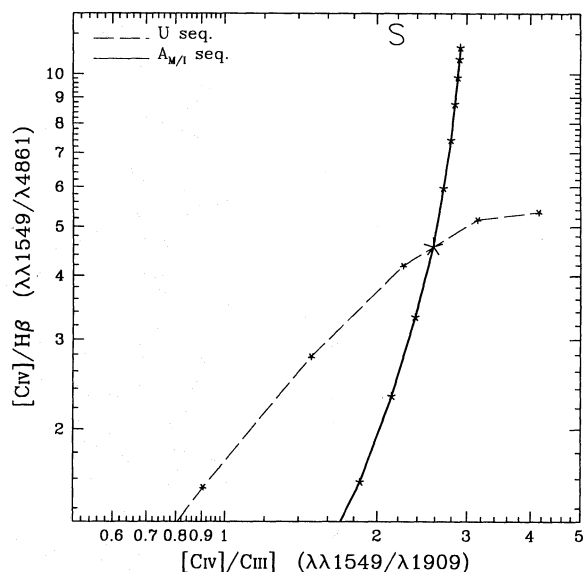the shock dominates over collisional ionization. Considering the conditions under which the photoionizing shock models of Sutherland et al. (1993) result in [O iii]/Hβ ratios in excess of 10, we find the same problems as in the standard photoionization model, since the shock simply generates the ionizing photons. One would presumably have to consider photoionization of MB clouds by shocks to resolve this problem.

Another interesting aspect to consider is the expected temperature for the IB component as measured by the ratio R_{NII}=[N ii]λ5755/[N ii]λ6583. Since the MB component emits negligible [N ii] as can be inferred from Table 2, the ratio R_{NII}=0.013 characterizing the IB component applies essentially to the whole A$_{M/I}$-sequence. This corresponds to T_{NII}=9 200 K, which is consistent with the measured temperature of 10 000 $\pm$ 600 K in the NW knot of Cyg A (Tadhunter et al. 1994). We emphasize that a general characteristic of the U-sequence (adopting U$\leq$0.01) is that the T_{OIII} temperature is only slightly higher (by *less* than 1 000 K) than the T_{NII} temperature, while our A$_{M/I}$-sequence predicts a much higher temperature difference of 5 000 K, in agreement with the observations of Tadhunter et al. (1994).

4.5. Miscellaneous aspects

4.5.1. LINERs revisited

AGN with low ionization spectra and classified as LINERs (Heckman 1980) are still difficult to comprehend. Many different and opposing models have been proposed over the years. One difficulty of models involving photoionization by a nuclear source is that such sources are often not seen (Maoz et al. 1995; Eracleous et al. 1995). The difficulty of the models is not in reproducing the emission line spectra but in pinning down the
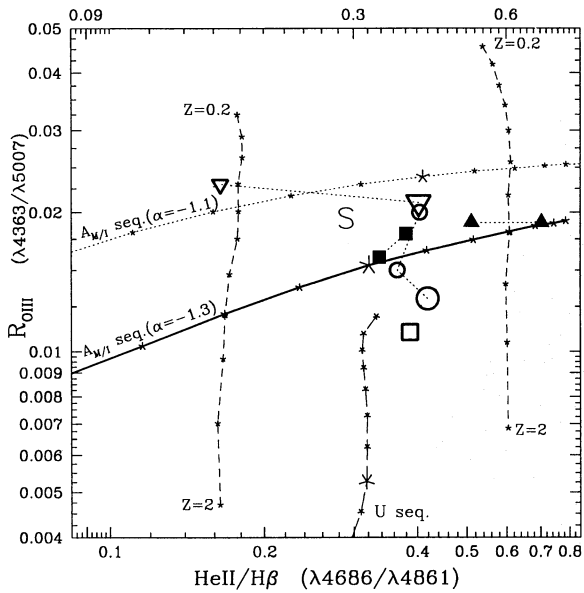
Fig. 12. Diagram of the line ratios R_{OIII} (4363Å/5007Å) against He II/Hβ. The symbols have the same meaning as in Fig. 5. $A_{M/I}$ is *increasing* from left to right. The two short-dash lines correspond to metallicity sequences ($0.2 \leq Z \leq 2.0$) at $A_{M/I} = 0.4$ (left) and 4.0 (right), respectively ($\alpha = -1.3$). The asterisks indicate steps of 0.1 dex in Z. The dotted line represents a solar metallicity $A_{M/I}$-sequence calculated with a larger pressure jump ($P_{IB}/P_{MB} = 40$) and a harder continuum ($\alpha = -1.1$).

Fig. 13. Diagram of the line ratios [N II]/[O II] against [O II]/[O III]. The symbols have the same meaning as in Fig. 5. $A_{M/I}$ is *decreasing* from left to right. The two short-dash lines correspond to metallicity sequences ($0.2 \leq Z \leq 2.0$) at $A_{M/I} = 4.0$ (left) and 0.4 (right), respectively. The asterisks indicate steps of 0.1 dex in Z.

excitation mechanism. The ideas proposed so far range from stellar or nuclear photoionization to shocks. In the category of models consisting of (steady-state) photoionization by a nuclear power law UV source, two models have been proposed and are broadly successful in explaining the low ionization level observed. On the one hand, Ferland & Netzer (1983) proposed a slab photoionized by a power law but with a very low ionization parameter, while on the other, Halpern & Steiner (1983) proposed a scheme in which the ionizing energy is partially absorbed by broad line clouds which subtend a covering factor f at the nuclear source. Halpern & Steiner (1983) indicated that the modification of the ionizing spectrum by the absorber resulted in a line spectrum little different from that obtained by simply reducing U by a factor f. We argue that the He II/Hβ ratio would be strongly affected in such a scenario. The ionizing spectrum illuminating the IB component in our model shares many similarities with the absorbed continuum proposed by Halpern & Steiner (1983) for LINERs, although in our case we propose that MB clouds (hidden from view by obscuring material: Fig. 4) instead of BLR clouds are the absorber. Whatever the nature of the absorber, we expect very similar effects on the continuum for a given value of F_{MB}, namely a deeper absorption trough above the threshold of He$^+$ than that of H$^\circ$ (e.g. Ferland et al. 1996).

The motivation for applying the $A_{M/I}$-sequence to LINERs stems from the fact that the sequence tends towards the position occupied by LINERs ("L") in Figs. 5 and 6. One prediction
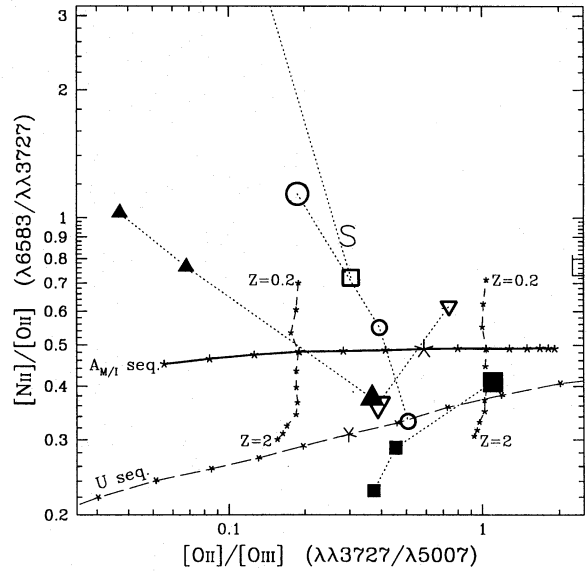
of our absorber model of LINERs is a ratio He II/Hβ<0.01 (IB spectrum in Table 2) while the value calculated for a pure power law exceeds 0.15, as shown by Ferland & Netzer (1983). The fact that no reliable detection of the He II line in bona fide LINERs has been reported suggests that there could be a serious problem with the popular picture of simply reducing U in a standard power-law photoionization model. In cooling flow galaxies, the emission line filaments produce a low excitation spectrum which we suggest could also be the result of nuclear photoionization by an absorbed power law rather than by the surrounding hot X-ray gas. In the cD galaxy in the cluster Abell 2597, a measurement by Donahue (private communication) indicates He II/H$\beta\leq$0.05 which is lower than expected for a pure power law or a hot, X-ray emitting gas.

4.5.2. The [N II]/[O II] problem discussed by VGDP

VGDP have studied the loci of hybrid (shock-photoionization) models in various line ratio diagrams. Such models are successful in accounting for temperatures up to R_{OIII}=0.06, but result in a much higher [N II]/[O II] ratio than the mean value observed in EELR. VGDP argued in favour of a reduction of the N/O metallicity ratio by a factor 4. Although such N/O underabundance can be justified under certain scenarios of stellar activity, it is interesting to note that pure photoionization with solar metallicity is equally successful for the objects in our sample. This is shown in Fig. 13 in which we use the same axes as in VGDP. Our mean calculated value is also very similar to that of [N II]/[O II] $\simeq$ 0.43 calculated by VP92 (see solid line in the Fig. 7 of VP92) who used solar N/O and pure photoionization.

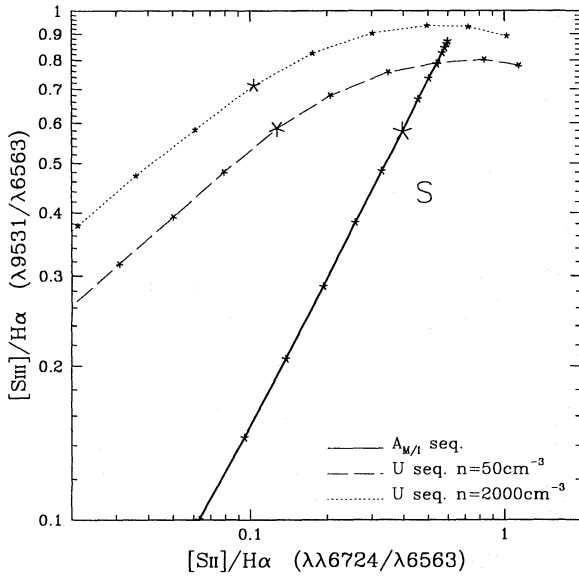**Fig. 14.** Diagram of the line ratios [S III]/Hα against [S II]/Hα. The symbols have the same meaning as in Fig. 5. $A_{M/I}$ is *decreasing* from left to right. The dotted line represents a U-sequence with a higher density of $2\,000\,\mathrm{cm}^{-3}$, comparable to the density within the IB component

The sample in VGDP, however, is much larger and clearly some extended gas regions have very low [N II]/[O II]. For these objects, the N/O ratio is probably underabundant. In Fig. 13 the short-dash lines indicate the effect of varying Z (but keeping constant N/O).

4.5.3. Internal dust and the infrared [Ca II] lines

We have not explored in detail the effect of varying the dust content which is quite low in the current models ($\mu = 0.015$). We found, however, through various experiments, that internal dust had a much more drastic effect on the MB component than on the IB component. For instance, with $\mu_{MB}=0.15$, the geometrical thickness of the MB component (for the same F_{MB}) was significantly reduced and its temperature increased. In the case of the IB component, on the other hand, a test with $\mu_{IB}=0.30$ showed that the emission line spectrum is only slightly changed. The reason is that within the fully ionized region the dust opacity ratio of the IB component relative to MB is given by $\mu_{IB}N_{IB}^{H^+}/\mu_{MB}N_{MB}^{H^+} \sim 0.05$ (cf. Eqs. 3 and 4).

Since the nondetection of the [Ca II]$\lambda7291$ line is generally interpreted as being the result of depletion of Ca unto dust (Kingdon et al. 1995; Villar-Martín & Binette 1996), substantial amounts of dust within the IB slab would suffice to reduce the predicted intensity to the observed upper limits, yet alter only slightly the other IB line ratios.

4.5.4. The [S III]$\lambda9531$ line

The near-infrared lines are now available for a reasonable sample of Seyfert galaxies following the work of Osterbrock et al. (1992). One reported problem with photoionization models is

the strength of the [S III]$\lambda9531$ line, which is predicted to be much stronger than observed. Although our models are designed for low density objects, it remains interesting to present a diagram (Fig. 14) showing the locus of the $A_{M/I}$-sequence and the mean ratio ('S') observed by Osterbrock et al. (1992). The current calculations are *not* inconsistent with a solar S/O abundance ratio, which is encouraging. If instead of $n=50\,\mathrm{cm}^{-3}$, the higher density of $2\,000\,\mathrm{cm}^{-3}$ (which is more comparable to the density characterizing the IB component plotted in Fig. 14) is used in the U-sequence, the discrepancy with the data would get worse, as shown by the dotted line in Fig. 14.

5. Conclusions

5.1. New results

1. We have discovered a correlation between the excitation of the ionized gas defined by ratios like [O II]/[O III] (3727Å/5007Å) or [O II]/[Ne V] (3727Å/3426Å), and He II/Hβ. The standard U-sequence is incompatible with such correlations. Diagrams based on He II/Hβ constitute an unequivocal discriminant between the models presented here and a traditional U-sequence. In other traditional diagrams (e.g. BPT), the two sequences are otherwise quite similar.

2. We have shown that the temperature problem and the underprediction of C IV and [Ne V] lines can now be solved using a matter-bounded component which is subjected to a high intensity ionization field ($U_{MB}\gg0.01$). In our $A_{M/I}$-sequence, the low excitation lines are produced by the ionizing radiation escaping from the MB component. We have shown that we expect a much lower temperature - by as much as $5\,000$ K - from the [N II] lines (R_{NII}) than from the [O III] lines (R_{OIII}).

3. We consider that the truncation of the MB clouds coincides with the exhaustion of the He$^+$ ionizing photons and that the IB clouds are of lower excitation due to the much lower radiation pressure exerted by the filtered continuum.

4. Measurement of the He II/Hβ ratio is fundamental to further our understanding of the extended ionized gas in AGN. It is particularly important to measure this ratio in LINERs or 'cooling flows' if we wish to distinguish between the wide range of interpretations proposed so far.

5.2. Future directions

In this paper we have explored the consequence of a model in which the ionization-bounded component sees a spectrum modified by absorption within the matter-bounded component. A next step should consider (more) internal dust and the use of a harder continuum impinging on the MB component. Could for instance an ionizing energy distribution as hard as that studied by Reynolds & Fabian (1995) or Ferland et al. (1996) reproduce the NLR spectrum? Radiation pressure is probably of great importance to the dynamics of the matter-bounded clouds. Hydrodynamical models should address this issue by taking into

account the differing heating function and opacity at high values of U from those at low values.

Since the successfull resolution of the three problems discussed in Sect. 1.2 requires matter-bounded clouds of the *appropriate* thickness (cf. Sect. 2.2), further studies by hydrodynamicists are needed to investigate whether an explanation exists for such preferred cloud's structure.

Observations with large aperture telescopes will be necessary if we hope to detect or set stringent limits on the value of the He II/Hβ ratio in LINERs (& cooling flows) given the very low contrast of such weak emission lines against the underlying stellar continuum. Similarly, measurement of the weak [N II]λ5755 line from extended ionized regions of moderate to high excitation will be crucial for confirming the validity of the MB/IB dual-component approach developed in this paper.

References

Aggarwal, K. M., Berrington, K. A., Burke, P. G., Kingston, A. E., 1991, J. Phys. B. 24, 1385

Anders, E., Grevesse, N., 1989, Geochim. Cosmochim. Acta 53, 197

Baldwin, J. A., Phillips M. M., Terlevich, R., 1981, PASP 93, 5 (BPT)

Baldwin et al., 1991, ApJ 374, 580

Bergeron, J., Petitjean, P., Durret, F., 1989, A&A 213, 61

Bertoldi, F. 1989, ApJ, 346, 735

Bertoldi, F., McKee, C. F. 1990, ApJ, 354, 529

Binette, L., Robinson, A., Courvoisier, T. J. L., 1988, A&A 194, 65

Binette, L., Courvoisier, T. J. L., Robinson, A., 1988, A&A 190, 29

Binette, L., Wang, J. C. L., Zuo, L., Magris, C., M., 1993a, AJ 105, 797

Binette L., Wang, J., Villar-Martín, M., Martin, P. G., Magris C., M., 1993b, ApJ 414, 535

Cameron, M., et al., 1993, ApJ 419 136

Contini, M., Viegas-Aldrovandi, S. M., 1989, ApJ 343, 78

DeRobertis, M. M., Osterbrock, D. E., 1984, ApJ 286, 171

DeRobertis, M. M., Osterbrock, D. E., 1986, ApJ 301, 727

Dopita, M. A., Sutherland, R. S., 1995, ApJ 455, 468

Dopita, M. A., Sutherland, R. S., 1996, ApJS 102, 161

Durret, F., 1990, A&A 229, 351

Eracleous, M., Livio, M., Binette, L., 1995, ApJL 445, L1

Evans, I. N., Dopita, M. A., 1986, ApJL 310, L15

Ferland, G. J., et al., 1996, ApJ in press

Ferland, G. J., Mushotzky, R. F., 1982, ApJ 262, 564

Ferland, G., Netzer, H., 1983, ApJ 264, 105

Ferland, G. J., Osterbrock D. E., 1985, ApJ 300, 658 (FO86)

Filippenko, A. V., Halpern, J. P., 1984, ApJ 285, 458

Fosbury, R. A. E., 1989, in: ESO Workshop on Extranuclear Activity in Galaxies, eds Meurs, E. J. A., Fosbury, R. A. E., ESO Conf. and Workshop Proc. No. 32, Garching, p. 169

Halpern, J. P., Steiner, 1983, ApJL 269, L37

Haniff, C. A., Ward, M. J., Wilson, A. S., 1991, ApJ 368, 167

Heckman, T. M., 1980, A&A 87, 152

Ho, L. C., Filippenko, A. V., Sargent, W. L. W., 1993, ApJ 417, 63

Kingdon, J., Ferland, G. J., Feibelman, W.A., 1995, ApJ 439, 793

Magris C., G., Binette, L., Martin. P. G., 1993, in: The Nearest Active Galaxies, ed. J. Beckman, Astrophysics and Space Science 205, p. 141

Maoz, D., et al., 1995, ApJ 440, 91

Mathews, W. G., Ferland, G. J., 1987, ApJ 323, 456

McCarthy, P., 1993, ARA&A 31, 639

Morganti, R., Robinson, A., Fosbury, R. A. E., di Serego Alighieri, S., Tadhunter, C. N., Malin D. F., 1991, MNRAS 249, 91

Nazarova, L. S., 1995, A&A 299, 359

Osterbrock, D. E., Tran, H. D., Veilleux, S., 1992, ApJ 389, 196

Pelat, D., Fosbury, R. A. E., Alloin, D., 1981, MNRAS 195, 787

Péquignot, D., 1984, A&A 131, 159

Péquignot, D., Dennefeld, M., 1983, A&A 120, 249

Prieto, A., Walsh, J. R., Fosbury, R. A. E., di Serego Alighieri, S., 1993, MNRAS 263, 10

Reynolds, C. S., Fabian, A. C., MNRAS 273, 1167

Robinson, A., Binette, L., Fosbury, R. A. E., Tadhunter, C. N., 1987, MNRAS 227, 97 (RBFT)

Stasińska, G., 1984, A&A 135, 341 (ST84)

Storchi-Bergmann, T., Wilson, A. S., Mulchaey, J. S., Binette, L., 1996, A&A in press (Paper I)

Sutherland, R. S., Bicknell, G. V., Dopita, M. A., 1993, ApJ 414, 510

Tadhunter, C.N., 1986, D.Phil. Thesis, University of Sussex

Tadhunter, C. N., Fosbury, R. A. E., di Serego Alighieri, S., Bland, J., Danziger, J., Goss, W. M., McAdam, W. B., Snijders, M. A. J., 1988, MNRAS 235, 403

Tadhunter, C. N., Robinson, A., Morganti, R., 1989, in: ESO Workshop on Extranuclear Activity in Galaxies, eds Meurs, E. J. A., Fosbury, R. A. E., ESO Conf. and Workshop Proc. No. 32, Garching, p. 293 (TRM89)

Tadhunter, C. N., Metz, S., Robinson, A., 1994, MNRAS 268, 989

Unger, S. W., Pedlar, A., Axon D. J., Whittle, M., Meurs, E. J. A., Ward, M. J., 1987, MNRAS 228, 671

Veilleux, S., Osterbrock, D. E., 1987, ApJS 63, 295

Viegas, S. M., 1988, ApJL 330, L9

Viegas, S. M., de Gouveia Dal Pino, E. M., 1992, ApJ 384, 467 (VGDP)

Viegas, S. M., Gruenwald, R. B., 1988, ApJ 324, 683

Viegas, S. M., Prieto, A., 1992, MNRAS 258, 483 (VP92)

Villar-Martín, M., Binette, L., Fosbury, R. A. E., 1996, A&A submitted

Villar-Martín, M., Binette, L., 1996, A&A in press

Wilson, A. S., 1979, Proc. Roy. Soc. (London) (A) 366, 461

Wilson, A. S., 1995, in: Evidence for the torus, Proc. of the Oxford astrophysics workshop, Aug. 30 - Sept. 2, 1994, Ed. M. J. Ward, p. 55 in press